Applied Soft Computing 41 (2016) 104–119

Contents lists available at ScienceDirect

Applied Soft Computing

journal homepage: www.elsevier.com/locate/asoc

Modified possibilistic fuzzy C-means algorithms for segmentation of magnetic resonance image

Jeetashree Aparajeeta *, Pradipta Kumar Nanda, Niva Das

Image & Video Analysis Lab, Department of Electronics and Communication Engineering, ITER, Siksha 'O' Anusandhan University, Bhubaneswar 751030, India

ARTICLE INFO

Article history:
Received 9 April 2015
Received in revised form
25 September 2015
Accepted 1 December 2015
Available online 4 January 2016

Keywords:
Magnetic resonance imaging
Bias field
Neighbourhood
Fuzzy C-means
Possibilistic C-means

ABSTRACT

The brain magnetic resonance (MR) image has an embedded bias field. This field needs to be corrected to obtain the actual MR image for classification. Bias field, being a slowly varying nonlinear field, needs to be estimated. In this paper, we have proposed three schemes and in turn three algorithms to segment the given MR image while estimating the bias field. The problem is compounded when the MR image is corrupted with noise in addition to the inherent bias field. The notions of possibilistic and fuzzy membership have been combined to take care of the modeling of the bias field and noise. The weighted typicality measure together with the weighted fuzzy membership has been used to model the image. The above resulted in the proposed Bias Corrected Possibilistic Fuzzy C-Means (BCPFCM) strategy and the algorithm. Further reinforcing the neighbourhood data to the modeling aspect has resulted in the two other strategies namely Bias Corrected Possibilistic Neighborhood Fuzzy C-Means (BCPNFCM) and Bias Corrected Separately weighted Possibilistic Neighborhood Fuzzy C-Means (BCSPNFCM). The proposed algorithms have successfully been tested with synthetic data with bias field of low and high spatial frequency. Noisy brain MR images with Gaussian Noise of varying strength have been considered from the BrainWeb database. The algorithms have also been tested on real brain MR data set with axial and sagittal view and it has been found that the proposed algorithms produced segmentation results with less percentage of misclassification errors as compared to the Bias Corrected Fuzzy C-Means (BCFCM) algorithm proposed by Ahmed et al. [4]. The performance of the proposed algorithms has been compared with algorithms from other paradigm in the context of Tanimoto's index.

1. Introduction

Intensity inhomogeneity poses a challenge in MR image segmentation. It appears as a slowly varying nonlinear field in MR images, known as the bias field, that changes the tissue statistics. Because of bias field, intensity of pixels of a particular class at other locations appears to belong to different classes. The conventional segmentation methods fail to classify such tissue classes affected by intensity inhomogeneity. However the bias field changes from frame to frame for a particular patient and also from patient to patient in the same MR system. To handle such problems, there is a need to model the nonlinear bias field to control the effect of nonlinearity so that tissue properties can be retained leading to accurate classification.

It is known from literature that fuzzy-C means algorithm [1] has proved to be an efficient tool to model the uncertainty in the data set and achieve clustering. The limitations of FCM have been circumvented by Possibilistic FCM for clustering [2,3]. Fuzzy C means and its variants have been proposed in the literature to estimate the bias field and segment the brain MR images. The major limitations of these methods are: (i) sensitivity to number of clusters and choice of initial cluster centers, and (ii) mis-classification of different tissue classes in presence of noise and incorrect bias field estimation. But possibilistic partition depends upon the degree of compatibility or typicality, which some times give rise to coincident clusters. By and large, attempts have been made to accurately estimate the bias field [4] and thereafter subtracting the same from the original MR image to obtain bias free MR image for tissue identification. Many researchers over last one and half decade have modeled bias field as a multiplicative field in the observed MR image and have proposed novel strategies to obtain bias field and MR image segmentation. Even though there have been several existing algorithms, it remains a challenge to accurately estimate the bias field and the MR image segmentation.

The objective of this research is to estimate the bias field and classify different tissue classes of brain MR images. Furthermore, the brain MR data has an embedded nonlinear field, the bias field, that makes the problem more compounded. Therefore, attempts have been made to propose novel algorithms in possibilistic and fuzzy framework to take care the bias field in MR data. In order to address the above issues, we have proposed three modified FCM algorithms to estimate the bias field, segment the images, and thereby obtain bias corrected segmentation. This work is the extension of our previous work [5]. We have considered two cases, firstly the MR image with bias field and secondly noisy MR image with bias field. Both, the spatial inhomogeneity resulting from the bias field and the uncertainty due to noise, have been modeled using the notion of jointly handling the data with fuzziness and typicality of the data set. In order to deal with both the above issues, we have introduced the concept of weighted fuzzy membership and weighted typicality for both the pixel in consideration and its neighbourhood. The corresponding objective function yielded our first proposed algorithm known as Bias

* Corresponding author. Tel.: +91 9861160628.
E-mail addresses: j.aparajeeta@gmail.com (J. Aparajeeta), pknanda@soauniversity.ac.in (P.K. Nanda), nivadas@soauniversity.ac.in (N. Das).

http://dx.doi.org/10.1016/j.asoc.2015.12.003

Corrected Possibilistic FCM (BCPFCM). The fuzziness and typicality have specifically been considered for the neighbourhood pixels besides the pixel itself. This notion of differently reinforcing the neighbourhood pixel resulted in the algorithm namely Bias Corrected Possibilistic Neighborhood FCM (BCPNFCM). The fuzzy memberships and typicality measure have been considered separately for the neighbourhood pixels and the resulted algorithm is Bias Corrected Separately Weighted Possibilistic Neighborhood FCM (BCSPNFCM) algorithm. The updates of prototype, bias field, typicality and fuzzy memberships in all the three proposed algorithms have been found out. These updates have been used to estimate the bias field and the segmentation. The proposed algorithms could successfully be tested on synthetic images and also on real brain MR images from the BrainWeb database (brainweb.bic.mni.mcgill.ca/brainweb/) and from the IBSR database [6]. The results obtained by our proposed algorithms have been compared with that of BCFCM algorithm proposed by Ahmed et al. [4] where both bias field and segmentation has been obtained simultaneously. As regards segmentation accuracy, the performance of the proposed algorithms have been compared with algorithms from other paradigms in the context of Tanimoto's index and it has been observed the performance is comparable in some cases and in other cases the performance has been improved.

2. Related work

In brain MR images, different tissue classes can be separated based on the difference in their intensity labels. But due to the effect of the nonlinearity of bias field it changes the tissue properties and makes it difficult to segment them. Different clustering algorithms such as FCM [1], PCM [2] and PFCM [3], that take care of the uncertainty and typicality of the data, produce poor result in the presence of the nonlinear bias field in MR images. Variants of FCM algorithms are available with the neighboring effect and the notion of regularization. Pham and Prince [7] proposed a method by adding a first order and a second order regularization parameter and solved it using a multi-grid approach for faster implementation. Subsequently, Pham [8] proposed a spatial model with a regularized parameter which models the nonlinearity in MR images considering the neighbourhood memberships. Neighborhood membership forces a smoothing effect on fuzzy membership, providing a high correlation among the intensities that are close to each other and belongs to the same class. Belaroussi et al. [9] have presented an overview on methods for intensity inhomogeneity along with their validation and correction.

The neighbourhood intensities have been appropriately weighted [4] which helps in obtaining piece wise homogeneous solution and has proved to be effective for MR images with salt and pepper noise. Though this model produces a proper estimate of bias field and segmentation, it has been found to be sensitive to the associated parameters. In order to enhance the efficiency in the presence of noise, Zhao et al. [10] have redefined the model by incorporating the non-local spatial information. Szilagy et al. [11] proposed a modification of FCM with application of local filtering to each voxel and thereafter introduced a new factor to reduce computation. Bias field has also been modeled by Liew and Yan [12] as a stack of smoothing B-Spline surfaces and has redefined the dissimilarity index considering the local spatial continuity constraint in traditional FCM. Two regularization parameters have been added to ensure the smoothing of B-Spline surfaces. This new dissimilarity index considers the neighbourhood effect adaptively. It has been observed that the dissimilarity measure has further been modified by Chen and Zhang [13] where the Euclidean norm of FCM and BCFCM algorithms have been replaced with non-Euclidean kernel induced dissimilarity measure. The effect of kernel induced dissimilarity measure makes the algorithm robust against noise as compared to Euclidean norm at the cost of computational complexity. The dissimilarity measure proposed by Chen and Zhang [13] has further been modified by Liao et al. [14] using Gaussian radial basis function.

The objective function proposed by Chen and Zhang [13] has been modified by Chen et al. [15] with a linear combination of multiple kernels. The notion of neighbourhood has been introduced to the proposed method of Chen and Zhang [13] by Xu and Ohya [16]. The dissimilarity index of FCM has further been modified by Shen et al. [17] with a weighted Euclidean norm, where the weight is a function of neighbourhood feature. Subsequently, Wang et al. [18] modified the FCM distance function as weighted sum of distance influenced by local and non-local information that resulted in improved segmentation with increase in computational complexity. Bias field has been modeled differently by different authors. It has been modeled as: (i) cubic spline by Salvado and Wilson [19], and (ii) weighted sum of singularity functions by Luo et al. [20]. By and large, the bias field has been considered as a multiplicative field in the MR image model, particularly Siyal and Yu [21] have modeled the bias as the multiplicative field where they have smoothened the bias field using the mean spread filter and used fuzzy filter for noise removal.

Another approach, proposed by Szilagyi et al. [22,23], has defined a complex filter as the pre-processing filter to reduce the bias field effect and this filter also extracted relevant features thus making the resulting image to respond to clustering effectively. Entropy based cost function has been proposed by Manjon et al. [24] for considering image intensity and gradient information. Gray level histogram information and spatial information through B-Spline has been considered by Milles et al. [25]. Verma et al. [26] proposed a variational level set approach for both additive and multiplicative intensity inhomogeneity correction. Over the years, different researchers such as Ji et al. and Szilagyi et al. [27,28] proposed different methods using both fuzzy and typicality to model bias field.

3. MR image model

The MR image consists of different tissue classes, such as Gray Matter (GM), White Matter (WM) and Cerebro Spinal Fluid (CSF) with embedded bias field. Let X denote the tissue classes and B is the bias field and Y is the observed MR image. We have modeled the MR image X with B as a multiplicative field that varies slowly across the observed image and the model is given by,

$$Y = XB \tag{1}$$

Taking Logarithm of both sides of (1) results in,

$$\log(Y) = \log(X) + \log(B)$$

$$y = x + \beta \tag{2}$$

4. Background work

It is known that FCM and PCM algorithms have limitation in clustering a data set having outliers and also in estimating the bias field of MR images. Ahmed et al. [4] proposed a method for bias field (intensity inhomogeneity) compensation by taking into account the effect of neighboring pixels. The proposed algorithm is the modified version of the standard FCM with a regularizer. The neighbourhood labeling acts as a regularizer and biases the solution toward piece wise homogeneous solution. This helps to reduce the effect of noise and bias field on segmented output. The objective function is given as follows,

$$J_m = \sum_{i=1}^{c}\sum_{j=1}^{p} u_{ij}^m \|y_j - \beta_j - v_i\|^2 + \frac{\alpha}{N_r}\sum_{i=1}^{c}\sum_{j=1}^{p} u_{ij}^m \left(\sum_{r \in N_k} \|y_r - \beta_r - v_i\|^2\right) \tag{3}$$

where J_m denotes the objective function, v_i is the ith cluster prototype, N_k is the set of neighbourhood pixels of y_j, N_r is the cardinality

$X_{i-1,j-1}$	$X_{i-1,j}$	$X_{i-1,j+1}$
$X_{i,j-1}$	$X_{i,j}$	$X_{i,j+1}$
$X_{i+1,j-1}$	$X_{i+1,j}$	$X_{i+1,j+1}$

(a)

$t_{i-1,j-1}$	$t_{i-1,j}$	$t_{i-1,j+1}$
$t_{i,j-1}$	$t_{i,j}$	$t_{i,j+1}$
$t_{i+1,j-1}$	$t_{i+1,j}$	$t_{i+1,j+1}$

(b)

$u_{i-1,j-1}$	$u_{i-1,j}$	$u_{i-1,j+1}$
$u_{i,j-1}$	$u_{i,j}$	$u_{i,j+1}$
$u_{i+1,j-1}$	$u_{i+1,j}$	$u_{i+1,j+1}$

(c)

Fig. 1. Proposed Idea (BCPFCM).

of N_k, u_{ij} is the fuzzy membership and the parameter α controls the neighbourhood. Further, c denotes the number of centers where as p denotes the number of pixels in the given image.

5. Bias Corrected Possibilistic FCM (BCPFCM) strategy

The source MR image could be contaminated with noise besides the inherent embedded nonlinear field, the bias field. In the objective function as given in (3), fuzzy membership function has been assigned to every pixel as well as the neighbourhood pixels. In order to deal with the non-linearity associated with the neighbourhood pixels and the pixel itself, we weigh the distance functions of the pixel considered and the neighbourhood pixels by a weighted linear combination of the fuzzy and typicality memberships (u_{ij}, t_{ij}). Isolated data points and noisy data points have been taken care using the notion of typicality and hence we have modeled the noisy bias field data using the notion of typicality. The notion behind the development of the objective function has been depicted through Fig. 1. In Fig. 1(a) a window housing the neighbourhood pixels together with the pixel itself has been presented. These data points have been modeled jointly with the typicality measure and fuzzy membership values. Fig. 1(b) and (c) shows the corresponding templates of typicality and fuzziness. These two templates have been appropriately weighted by the weighting parameters. The distances between neighboring pixels from the cluster prototype have been weighted by the joint effect of weighted typicality and fuzziness. Because of relaxing the constraint on the typicality measure, a penalty term has been added and thus the complete objective function evolved taking care of efficient modeling of the data. The objective function is given in (4).

The first term of this objective function (4) weighs the distance function D_{ij} with sum of weighted membership function of the pixel and also the typicality of pixel. The typicality of the neighbourhood pixels has been taken care by the second term. The fuzzy membership values of the neighboring pixels have also been incorporated in this term. Further, the second term with weighted typicality and fuzzy memberships can take care of the spatial inhomogeneity of the data in the neighbourhood. This second term also serves as a regularizer of the objective function. Thus, both the typicality and fuzzy membership of the neighbourhood pixels account for the spatial inhomogeneity resulting from the bias field. The following objective function is minimized with the constraint $\sum_{i=1}^{c} u_{ij} = 1$.

$$J_{\mathrm{BCPFCM}} = \sum_{i=1}^{c}\sum_{j=1}^{p}(au_{ij}^{m} + bt_{ij}^{n})D_{ij} + \frac{\alpha}{N_r}\sum_{i=1}^{c}\sum_{j=1}^{p}(au_{ij}^{m} + bt_{ij}^{n})\gamma_i + \sum_{i=1}^{c}\eta_i\sum_{j=1}^{p}(1-t_{ij})^{n} \tag{4}$$

where $D_{ij} = \|y_j - \beta_j - v_i\|^2$, $\gamma_i = \sum_{r \in N_k}\|y_r - \beta_r - v_i\|^2$, u_{ij} and t_{ij} are fuzzy and possibilistic membership respectively, c is the number of clusters, p is the number of pixels, N_r is the number of neighbourhood pixels existing in a 3×3 window around y_j, N_k is the set of neighboring pixels present in a 3×3 window around y_j, $a > 0$ and $b > 1$, $0 < \alpha < 1$ and η_i is the zone of influence of ith cluster. This constrained optimization problem has been recast using Lagrange multiplier as,

$$J'_{\mathrm{BCPFCM}} = J_{\mathrm{BCPFCM}} + \sum_{j=1}^{p}\lambda\left(1 - \sum_{i=1}^{c}u_{ij}\right) \tag{5}$$

where λ is the Lagrangian constant. Hence, we minimize the following objective function with respect to u_{ij}, t_{ij}, v_i and β_{ij} to obtain the optimal estimates u_{ij}^*, t_{ij}^*, v_i^* and β_{ij}^*.

$$(u_{ij}^*, t_{ij}^*, v_i^*, \beta_{ij}^*) = arg \min_{(u_{ij}, t_{ij}, v_i, \beta_{ij})} J'_{\mathrm{BCPFCM}} \tag{6}$$

The zone of influence of a cluster as given by Krishnapuram and Keller [2] is given as,

$$\eta_i = \frac{\sum_{j=1}^{p} u_{ij}^{m} d_{ij}^{2}}{\sum_{j=1}^{p} u_{ij}^{m}} \tag{7}$$

Minimization of (6) has been achieved by gradient based notion. The zero gradient condition of the constraint resulted in the update equations for u_{ij}, t_{ij}, v_i, β_j and are as follows.

Since J'_{BCPFCM} has been regularized, gradients with respect to u_{ij}, t_{ij}, v_i and β_j can be computed and zero gradient condition results in the update equations of u_{ij}^*, t_{ij}^*, v_i^* and β_j^*. The derivations are given in Appendix A.

Thus, update equations for u_{ij}, t_{ij}, v_i, β_j are obtained with zero gradient of the function given by (5) and are as follows. The update equation for fuzzy memberships is given by,

$$u_{ij} = \frac{1}{\sum_{k=1}^{c}\left(\frac{D_{ij} + \frac{\alpha}{N_r}\gamma_i}{D_{kj} + \frac{\alpha}{N_r}\gamma_k}\right)^{\frac{1}{m-1}}} \tag{8}$$

The update equation for possibilistic memberships is,

$$t_{ij} = \frac{1}{1 + \left[\frac{b}{\eta_i}(D_{ij} + \frac{\alpha}{N_r}\gamma_i)\right]^{\frac{1}{n-1}}} \tag{9}$$

The update equation for cluster prototype is,

$$v_i = \frac{\sum_{j=1}^{p}(au_{ij}^{m} + bt_{ij}^{n})\|y_j - \beta_j\| + \frac{\alpha}{N_r}\sum_{j=1}^{p}(au_{ij}^{m} + bt_{ij}^{n})\sum_{r \in N_k}(y_r - \beta_r)}{\sum_{j=1}^{p}(au_{ij}^{m} + bt_{ij}^{n}) + \alpha\sum_{j=1}^{p}(au_{ij}^{m} + bt_{ij}^{n})} \tag{10}$$

The update equation for bias field is,

$$\beta_j = y_j - \frac{\sum_{i=1}^{c}(au_{ij}^{m} + bt_{ij}^{n})v_i}{\sum_{i=1}^{c}(au_{ij}^{m} + bt_{ij}^{n})} \tag{11}$$

With above updates of the parameters, the following algorithm has been proposed.

The salient steps of the algorithm are given below.

BCPFCMAlgorithm

Initialization:

Set β_j to zero, Threshold=0.5, initialize c and v_i.

Table 1
FCM.

(a) fuzzy membership with cluster center z=14

0.987499	0.999912	0.971873
0.579801	0.216605	0.006175
0.001074	0.971168	0.045936

(b) fuzzy membership with cluster center z=39

0.012501	0.000088	0.028127
0.420199	0.783395	0.993825
0.998926	0.028832	0.954064

Table 2
PCM.

(a) typicality membership with cluster center z=11

0.978024	0.706170	0.683893
0.063982	0.036337	0.015143
0.018571	0.255953	0.011215

(b) typicality membership with cluster center z=39

0.043832	0.053766	0.038646
0.159763	0.307445	0.944467
0.948516	0.073088	0.482846

1. Compute η_i using (7)
2. Compute Fuzzy membership as in (8) and Possibilistic membership as in (9)
3. Update cluster prototype as in (10)
4. Estimate the bias field as in (11) and compute the $\|v_{new} - v_{old}\|$
5. Repeat step $2 - 4$, until $Threshold > \|v_{new} - v_{old}\|$

The threshold for the stopping criterion has been chosen to be 0.5. The motivation behind choosing 0.5 is as follows. The cluster centers are the intensity values on the gray scale i.e. from 0 to 255. We expect a converged cluster center to be one of the discrete intensity values. Although our simulation takes care of floating point numbers, in order to avoid the computation for all the values between two consecutive discrete values, we have chosen the threshold for the stopping criterion as 0.5. Thus, the convergence clusters will be one of the discrete intensity gray values. Fixing a value lower than 0.5 would increase the computational time.

For the sake of illustration, we have considered a two class data window as shown in Fig. 2. Tables 1 and 2 show the fuzzy memberships and the typicality values obtained for this data window with the cluster centers $z = 14$, where z denotes the cluster center. As observed, FCM algorithm resulted in two cluster centers at 14 and 39. Based on the memberships and prototypes, the two classes have been highlighted. In case of PCM, the two classes are different from that of FCM. For example, the data point with a value of 26 have been clustered with 14 in FCM, while in PCM this has been clustered with 39. This is because of the change in the cluster center to 11 in PCM. Tables 3 and 4 shows the fuzzy memberships and typicality values obtained using the proposed BCPFCM algorithm. It can be observed from Tables 3 and 4 that typicality and fuzzy memberships resulted two identical cluster centers where as independent application of FCM and PCM give rise to three

11	14	09
26	31	42
39	18	47

Fig. 2. Data matrix.

Table 3
BCPFCM fuzzy membership.

(a) Fuzzy membership with cluster center z=14

0.999090	0.990937	0.863492
0.606917	0.327380	0.007934
0.039273	0.935755	0.145836

(b) Fuzzy membership with cluster center z=39

0.000910	0.009063	0.136508
0.393083	0.672620	0.0.992066
0.960727	0.064245	0.854164

Table 4
BCPFCM typicality membership.

(a) Typicality membership with cluster center z=14

0.999978	0.995263	0.398903
0.097245	0.035129	0.014990
0.016408	0.786843	0.014580

(b) Typicality membership with cluster center z=39

0.016641	0.016900	0.012635
0.040916	0.113902	0.988295
0.832159	0.018901	0.999998

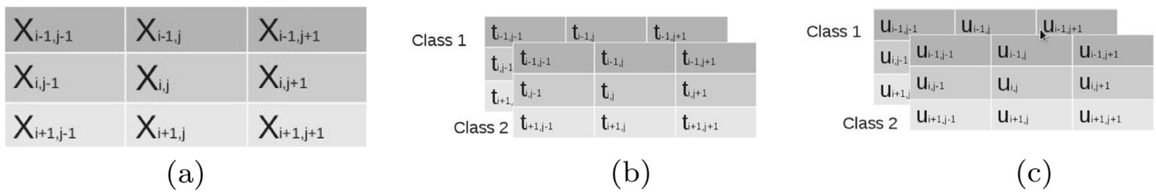

Fig. 3. Proposed Idea (BCPNFCM).

cluster centers. However, the joint weighted effect has resulted in two clusters.

6. Bias Corrected Possibilistic Neighborhood FCM (BCPNFCM) strategy

In this proposed scheme, we have considered both the typicality and fuzzy memberships in intra and interclass neighbourhoods. Fig. 3(a) shows a window with data points for a two class problem and the corresponding typicality measures for both the classes have been shown in Fig. 3(b). We have considered a single MR image having different cases. Since it is a two class problem, every pixel will belong to a class with some typicality value. So the whole image will have two sets (size of each set is same as image) of typicality values. The first set belonging to the first class and the second set belonging to the second class. These two sets are shown as two temporal frames in Fig. 3(b). However, these two sets are for a given MR image. Hence temporal frames do not correspond to different images (slices) rather to a single slice (frame). The interaction of a given typicality value corresponding to one class with the typicality values of the neighboring pixels of the second class is known as temporal interactions. The interaction of a given typicality value of a pixel of a given class with the neighboring pixels of the same class is known as spatial interaction. Thus, the combined interaction, both spatial and temporal, is known as spatiotemporal interaction. These, for ease of reference, have been arranged as two frames corresponding to two classes. This interaction has been referred to as spatiotemporal interactions and has contributed to the objective function. Similarly, every pixel will have a membership value for a particular class i.e. here class 1 and class 2. Thus these two sets of fuzzy membership values have been shown as two frames and the interaction among them is referred to as spatiotemporal interactions.

Analogously, Fig. 3(c) shows the fuzzy memberships of two possible classes. In this scheme, we weigh the neighbourhood pixels of different classes. Further, for a given data point, we consider the spatial neighbourhood of all the different classes. Implicitly, the effect of neighbourhood in spatial as well as temporal directions has been considered. This implicit spatiotemporal embedding is expected to take care of the existing nonlinearity in intraclass and interclass. Additionally, in the second term of (12), the terms of the inner sum correspond to the local memberships of the neighborhood pixels. Thus, the second term in totality takes care of the local and global effect of the memberships.

In (12), besides providing fuzziness and typicality to the associated pixel, we assign fuzziness and typicality to the distance function γ_i for each neighboring pixels. The combined effect is expected to regularize the objective function and augment the convergence of optimal solution. As usual, a penalty term has been added for the typicality measure to take care of the relaxation of the typicality constraints. This additional weight further reinforces the modeling of the bias field and noises.

However the fuzzy constraint remain the same. The following objective function has been minimized with the constraint $\sum_{i=1}^{c} u_{ij} = 1$.

$$J_{\text{BCPNFCM}} = \sum_{i=1}^{c}\sum_{j=1}^{p}(au_{ij}^{m} + bt_{ij}^{n})D_{ij} + \frac{\alpha}{N_r}\sum_{i=1}^{c}\sum_{j=1}^{p}\left(au_{ij}^{m} + bt_{ij}^{n}\right) \times \left(\sum_{l\in N_c}\sum_{s\in N_k}(au_{ls}^{m} + bt_{ls}^{n})\right)\gamma_i + \sum_{i=1}^{c}\eta_i\sum_{j=1}^{p}(1-t_{ij})^{n} \quad (12)$$

where $D_{ij} = \|y_j - \beta_j - v_i\|^2$, $\gamma_i = \sum_{r\in N_k}\|y_r - \beta_r - v_i\|^2$, N_c is the set of neighboring clusters excluding the current cluster and all other parameters carry the same meaning as defined in the previous proposed algorithm. Zero gradient condition results in updates of u_{ij}, t_{ij}, v_i, β_j.

$$J'_{\text{BCPNFCM}} = J_{\text{BCPNFCM}} + \sum_{j=1}^{p}\lambda\left(1 - \sum_{i=1}^{c}u_{ij}\right) \quad (13)$$

where λ is the Lagrangian constant. Hence, we minimize the following objective function with respect to u_{ij}, t_{ij}, v_i and β_{ij} to obtain the optimal estimates u_{ij}^*, t_{ij}^*, v_i^* and β_{ij}^*.

$$(u_{ij}^*, t_{ij}^*, v_i^*, \beta_{ij}^*) = arg \min_{(u_{ij}, t_{ij}, v_i, \beta_{ij})} J'_{\text{BCPNFCM}} \quad (14)$$

Using zero gradient condition, the update equations for u_{ij}, t_{ij}, v_i, β_j have been obtained. The following updates have been obtained along the similar lines as presented in Appendix A. The update equation for fuzzy memberships is,

$$u_{ij} = \frac{1}{\sum_{k=1}^{c}\left(\dfrac{D_{ij} + \frac{\alpha}{N_r}\gamma_i\left(\sum_{l\in N_c}\sum_{s\in N_k}(au_{ls}^{m} + bt_{ls}^{n})\right)}{D_{kj} + \frac{\alpha}{N_r}\gamma_k\left(\sum_{l\in N_c}\sum_{s\in N_k}(au_{ls}^{m} + bt_{ls}^{n})\right)}\right)^{\frac{1}{m-1}}} \quad (15)$$

The update equation for possibilistic memberships is,

$$t_{ij} = \frac{1}{1 + \left(\frac{b}{\eta}\left(D_{ij} + \frac{\alpha}{N_r}\gamma_i\left(\sum_{l\in N_c}\sum_{s\in N_k}(au_{ls}^{m} + bt_{ls}^{n})\right)\right)\right)^{\frac{1}{n-1}}} \quad (16)$$

The update equation for cluster prototype is found to be,

$$v_i = \frac{\sum_{j=1}^{p}(au_{ij}^{m} + bt_{ij}^{n})(y_j - \beta_j) + \frac{\alpha}{N_r}\sum_{j=1}^{p}(au_{ij}^{m} + bt_{ij}^{n})\left(\sum_{l\in N_c}\sum_{s\in N_k}(au_{ls}^{m} + bt_{ls}^{n})\right)\left(\sum_{r\in N_K}y_r - \beta_r\right)}{\sum_{j=1}^{p}(au_{ij}^{m} + bt_{ij}^{n}) + \alpha\sum_{j=1}^{p}(au_{ij}^{m} + bt_{ij}^{n})\left(\sum_{l\in N_c}\sum_{s\in N_k}(au_{ls}^{m} + bt_{ls}^{n})\right)} \quad (17)$$

The update equation for bias field has been found to be,

$$\beta_j = y_j - \frac{\sum_{i=1}^{c}(au_{ij}^{m} + bt_{ij}^{n})v_i}{\sum_{i=1}^{c}(au_{ij}^{m} + bt_{ij}^{n})} \quad (18)$$

Table 5
BCPNFCM fuzzy membership.

(a) Fuzzy membership with cluster center z=14

0.999429	0.991610	0.885036
0.629453	0.362626	0.014149
0.058389	0.936701	0.000170

(b) Fuzzy membership with cluster center z=44

0.000571	0.008390	0.114964
0.370547	0.637374	0.985851
0.941611	0.063299	0.999830

Table 6
BCPNFCM typicality membership.

(a) Typicality membership with cluster center z=14

0.957513	0.612978	0.979310
0.035362	0.017074	0.008461
0.008824	0.090214	0.008295

(b) Typicality membership with cluster center z=44

0.009842	0.010966	0.009603
0.033892	0.091779	0.968414
0.913456	0.018475	1.000000

The salient steps of the algorithm are given below.

BCPNFCMalgorithm

Initialization:

Set β_j to zero, Threshold=0.5, initialize c and v_i.

1. Compute η_i using (7)
2. Compute fuzzy membership as in [1] and Possibilistic membership as in [2]
3. Compute Fuzzy membership as in (15) and Possibilistic membership as in (16)
4. Update cluster prototype as in (17)
5. Estimate the bias field as in (18) and compute $\|v_{new} - v_{old}\|$
6. Repeat step $3 - 5$, until $Threshold > \|v_{new} - v_{old}\|$

The BCPNFCM algorithm has been applied on the same example considered earlier and the resulting membership and typicality values have been shown in Table 5 and Table 6 for two different cluster centers i.e. 14 and 44. The same example data set as given in Fig. 2 has also been considered. The cluster centers have been identified at 14 and 44. The fuzzy memberships have high value of memberships for the respective class of data. However, for cluster center at 14, the typical value for the data 26 is as low as 0.035. Similar result has also been found for the second class with the data point of 31.

7. Bias Corrected Separated Possibilistic Neighborhood FCM (BCSPNFCM) strategy

In this scheme, the neighbourhood pixel memberships have been considered separately and also weighted only with the respective membership. Analogously, the typicality in the neighbourhood has been considered separately and weighted by the respective typicality values only. This has been motivated to take care of the noises or isolated points in the neighbourhood and the spatial inhomogeneity due to the bias field.

The notion considered can also be explained using Fig. 3. Fig. 3(a) shows a window with data points. The notion of spatial interaction and spatiotemporal interaction is same as given in Section 7. The difference with the previous scheme is explained below. In this scheme, we consider the effect of typicality of neighborhood pixels and memberships of the neighborhood pixels separately. This has been considered besides jointly weighing with typicality and fuzzy membership. The separately weighted typicality is expected to take care of noise as well as isolated points. This has been reflected in the third and fourth terms of the objective function given by (19). These two terms reinforce the effect of neighborhood separately. In the third term of (19), the inner sum represents the effect of local fuzzy membership while the total term takes care of the local and global effects of fuzzy membership. Analogously, in the fourth term, the inner sum takes care of the local effect of typicality of the data while the total term takes care of local and global typicality effects.

Besides, these two terms serve as the regularization for the objective function. The combined effect of fuzzy membership and typicality of the neighbourhood has also been considered for strengthening regularization. This has resulted in efficient modeling of the data with uncertainty and hence resulted in the objective function given by (19).

The last term is penalty for the typicality of the data. Thus, the cost function of BCSPNFCM is given by,

Table 7
BCSPNFCM fuzzy membership.

(a) Fuzzy membership with cluster center z=12

0.988446	0.983167	0.988421
0.020663	0.021770	0.016686
0.005992	0.972233	0.005969

(b) Fuzzy membership with cluster center z=34

0.011554	0.016833	0.011579
0.979337	0.978230	0.983314
0.994008	0.027767	0.994031

Table 8
BCSPNFCM typicality membership.

(a) Typicality membership with cluster center z=12

0.983085	0.974831	0.983051
0.027462	0.027233	0.027244
0.027242	0.958745	0.027242

(b) Typicality membership with cluster center z=32

0.031030	0.031025	0.031030
0.977223	0.970708	0.977893
0.992477	0.031051	0.992508

$$J_{\mathrm{BCSPNFCM}} = \sum_{i=1}^{c}\sum_{j=1}^{p}\left(au_{ij}^{m}+bt_{ij}^{n}\right)D_{ij} + \frac{\alpha}{N_r}\sum_{i=1}^{c}\sum_{j=1}^{p}\left(au_{ij}^{m}+bt_{ij}^{n}\right)\gamma_i + \sum_{i=1}^{c}\sum_{j=1}^{p}au_{ij}^{m} \times\left(\sum_{l\in N_c}\sum_{s\in N_k}u_{ls}^{m}\right)\gamma_i + \sum_{i=1}^{c}\sum_{j=1}^{p}bt_{ij}^{n}\left(\sum_{l\in N_c}\sum_{s\in N_k}t_{ls}^{n}\right)\gamma_i + \sum_{i=1}^{c}\eta_i\sum_{j=1}^{p}\left(1-t_{ij}\right)^{n} \quad (19)$$

$$C = \frac{\sum_{j=1}^{p}\left(au_{ij}^{m}+bt_{ij}^{n}\right)(y_j-\beta_j)+\sum_{j=1}^{p}au_{ij}^{m}\left(\sum_{l\in N_c}\sum_{s\in N_k}u_{ls}^{m}\right)\left(\sum_{r\in N_k}(y_r-\beta_r)\right)}{(1+\alpha)\sum_{j=1}^{p}(au_{ij}^{m}+bt_{ij}^{n})+\sum_{j=1}^{p}au_{ij}^{m}\left(\sum_{l\in N_c}\sum_{s\in N_k}u_{ls}^{m}\right)+\sum_{j=1}^{p}bt_{ij}^{n}\left(\sum_{l\in N_c}\sum_{s\in N_k}t_{ls}^{n}\right)}$$

$$D = \frac{\frac{\alpha}{N_r}\sum_{j=1}^{p}(au_{ij}^{m}+bt_{ij}^{n})\left(\sum_{r\in N_k}(y_r-\beta_r)\right)+\sum_{j=1}^{p}bt_{ij}^{n}\left(\sum_{l\in N_c}\sum_{s\in N_k}t_{ls}^{n}\right)\left(\sum_{r\in N_k}(y_r-\beta_r)\right)}{(1+\alpha)\sum_{j=1}^{p}(au_{ij}^{m}+bt_{ij}^{n})+\sum_{j=1}^{p}au_{ij}^{m}\left(\sum_{l\in N_c}\sum_{s\in N_k}u_{ls}^{m}\right)+\sum_{j=1}^{p}bt_{ij}^{n}\left(\sum_{l\in N_c}\sum_{s\in N_k}t_{ls}^{n}\right)}$$

subject to constraint

$$\sum_{i=1}^{c}u_{ij}=1$$

where $D_{ij}=\|y_j-\beta_j-v_i\|^2$, $\gamma_i=\sum_{r\in N_k}\|y_r-\beta_r-v_i\|^2$, N_c is the set of neighboring clusters excluding the current cluster and all other parameters carry the same meaning as defined in the previous proposed algorithm. The minimization of the algorithm is achieved using Lagrange multiplier.

$$J'_{\mathrm{BCSPNFCM}} = J_{\mathrm{BCSPNFCM}} + \sum_{j=1}^{p}\lambda\left(1-\sum_{i=1}^{c}u_{ij}\right) \quad (20)$$

where λ is the Lagrangian constant. Hence, we minimize the following objective function with respect to u_{ij}, t_{ij}, v_i and β_{ij} to obtain the optimal estimates u_{ij}^{*}, t_{ij}^{*}, v_i^{*} and β_{ij}^{*}.

$$(u_{ij}^{*}, t_{ij}^{*}, v_i^{*}, \beta_{ij}^{*}) = arg\min_{(u_{ij},t_{ij},v_i,\beta_{ij})} J'_{\mathrm{BCSPNFCM}} \quad (21)$$

Using zero gradient condition, update equations for u_{ij}, t_{ij}, v_i, β_j have been obtained. The differentiation of the objective function J_{BCSPNFCM} with respect to u_{ij}, t_{ij}, v_i and β_j has resulted in the following prototypes. The following updates have been obtained along the similar lines as presented in Appendix A. The update equation for fuzzy membership is,

$$u_{ij} = \frac{1}{\sum_{k=1}^{c}\left(\frac{Dij+\frac{\alpha}{N_r}\gamma_i+\sum_{l\in N_c}\sum_{s\in N_k}u_{ls}^{m}\gamma_i}{Dkj+\frac{\alpha}{N_r}\gamma_k+\sum_{l\in N_c}\sum_{s\in N_k}u_{ls}^{m}\gamma_k}\right)^{\frac{1}{m-1}}} \quad (22)$$

and the update equation for possibilistic membership has been,

$$t_{ij} = \frac{1}{1+\left(\frac{b}{\eta_i}\left(D_{ij}+\frac{\alpha}{N_r}\gamma_i+\sum_{l\in N_c}\sum_{s\in N_k}t_{ls}^{n}\gamma_i\right)\right)^{\frac{1}{n-1}}} \quad (23)$$

The update equation for cluster prototype is found to be,

$$v_i = C + D \quad (24)$$

where

and the update equation for bias field has been found to be,

$$\beta_j = y_j - \frac{\sum_{i=1}^{c}(au_{ij}^{m}+bt_{ij}^{n})v_i}{\sum_{i=1}^{c}(au_{ij}^{m}+bt_{ij}^{n})} \quad (25)$$

The salient steps of the algorithm are given below.

BCSPNFCMalgorithm

Initialization:

Set β_j to zero, Threshold=0.5, initialize c and v_i.

1. Compute η_i using (7)
2. Calculate fuzzy membership as in FCM [1] and Possibilistic membership as in PCM [2]
3. Calculate Fuzzy membership as in (22) and Possibilistic membership as in (23)
4. Update cluster prototype as in (24)
5. Estimate the bias field as in (25) and compute $\|v_{new}-v_{old}\|$
6. Repeat step 3 − 5, until *Threshold* $> \|v_{new}-v_{old}\|$

For the same data points as given in Fig. 2, this algorithm resulted in two different cluster centers i.e. 12 and 34. Therefore, the two clusters are different from that of BCPNFCM algorithm. But in this case the typicality values are high for the respective classes. This algorithm has yielded appropriate fuzzy memberships and typicality values for pixels of different classes (Tables 7 and 8).

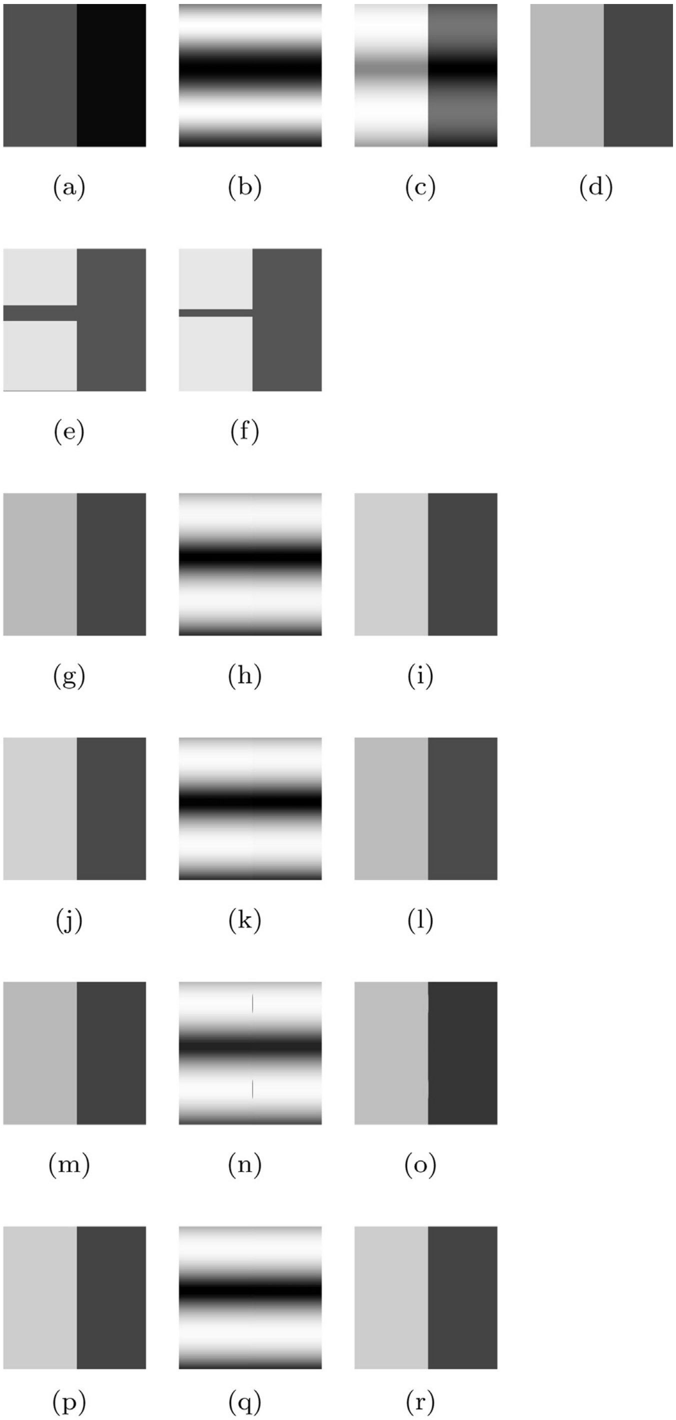

Fig. 4. Segmentation of synthetic images generated with low frequency bias field. (a) Original image, (b) 2D Bias, (c) synthetic image with bias, (d) ground truth, segmented image using, (e) FCM, (f) PFCM, (g–i) segmented image, estimated bias and bias corrected image using BCFCM, (j–l) segmented image, estimated bias and bias corrected image using BCPFCM, (m–o) segmented image, estimated bias and bias corrected image using BCPNFCM, (p–r) segmented image, estimated bias and bias corrected image using BCSPNFCM.

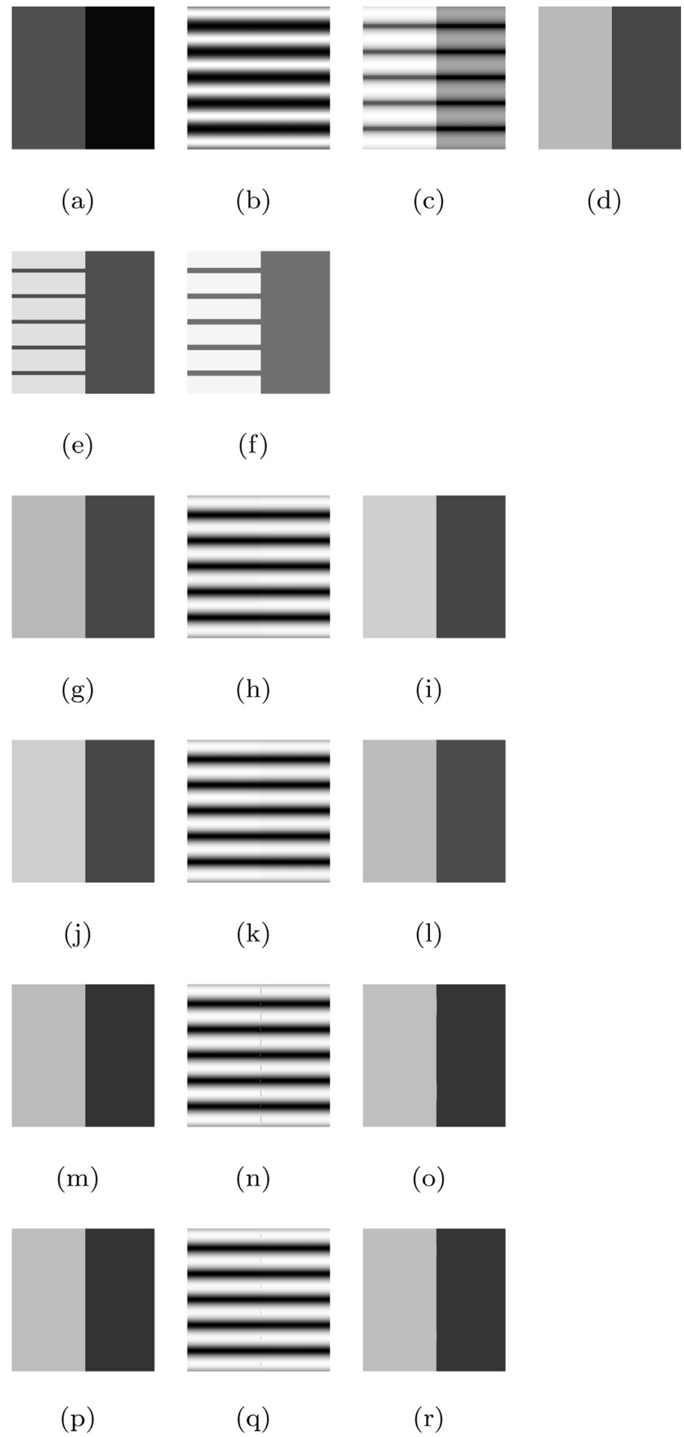

Fig. 5. Segmentation of synthetic images generated with low frequency bias field. (a) Original image, (b) 2D Bias, (c) ground truth, (d) synthetic image with bias, segmented image using, (e) FCM, (f) PFCM, (g–i) segmented image, estimated bias and bias corrected image using BCFCM, (j–l) segmented image, estimated bias and bias corrected image using BCPFCM, (m–o) segmented image, estimated bias and bias corrected image using BCPNFCM, (p–r) segmented image, estimated bias and bias corrected image using BCSPNFCM.

8. Results and discussions

The proposed algorithms have been tested on both synthetic as well as Brain MR images. The original synthetic image of two class is shown in Fig. 4(a) and two low spatial frequency signals, as shown in Figs. 4(b) and 5(b), have been added to the original image to result in two different observed images shown in Figs. 4(c) and 5(c). These two low spatial frequencies have been considered as the two bias fields. Two views of the brain MR images, namely the axial and sagittal view, have been considered. These views have been embedded with either the bias field or bias field plus noise. We have simulated in the Linux environment and the coding was developed in C-language. The Machine Specification is as follows: Dell

Table 9
Mis-classification error for synthetic data.

Algorithms	Synthetic-I (two cycle frequency) image (%)	Synthetic-II (high frequency) image (%)
FCM	5.79	7.08
PFCM	2.70	6.19
BCFCM	0.00	0.00
BCPFCM	0.00	0.00
BCPNFCM	0.0006	0.0006
BCSPNFCM	0.00	0.0006

Vostro, Intel Core i3-2310M Processor, 2.10 GHz×4 CPU, 2GB RAM and 32bit OS.

Synthetic images:

Fig. 4(a) shows the original synthetic image and Fig. 4(b) shows the image with a spatial sinusoidal signal having two cycles over the entire image. As mentioned earlier, the image of Fig. 4(b) serves as a bias field. Fig. 4(c) shows the image embedded with the bias field where the bias is clearly evident on this image. A ground truth has been constructed manually and has been shown in Fig. 4(d), which is in this case the original synthetic image.

Rest of the images shown in Fig. 4(e)–(r) are the segmented images, estimated bias field, and the bias corrected images obtained by the existing method and our proposed schemes. Fig. 4(e) and (f) shows the segmented images obtained by FCM and PFCM algorithms respectively and further it may be observed that the segmented images are not same as the ground truth images. The mid horizontal straps present in these two images lead to misclassification of pixels, that has been presented in Table 9. Fig. 4(g)–(r) shows the results obtained by different proposed schemes. The parameters used by different schemes have been presented in Table 10. It can be observed from Table 10 that the value of α is low, thereby indicating that the contribution of the neighbourhood pixels to the objective function is not very significant. It can be observed from Fig. 4(g)–(r) that the proposed algorithms could segment accurately and also estimate the bias field properly. This has also been reflected in Table 9. The percentage of mis-classification is defined as:

$$\text{Misclassification Error}(\%) = \frac{\text{No. of misclassified pixels}}{\text{Total no. of pixels}} \qquad (26)$$

The next example considered is the same synthetic two class image but with a bias field having higher spatial frequency (6 cycles). Spatial field is a sinusoidal signal having 6 cycles over the image. This sinusoidal field is the bias field and is shown in Fig. 5(b) and the image embedded with the bias field is shown in Fig. 5(c). The corresponding ground truth is shown in Fig. 5(d). The results obtained by FCM and PFCM algorithm are shown in Fig. 5(e) and (f), respectively, where it can be seen that the segmented images could not be free entirely from the bias field and hence increased the misclassification errors. The strips observed in the segmented image indicate the presence of the bias fields. Fig. 5(g)–(r) present different results obtained by the proposed schemes and the scheme by Ahmed et al. [4]. The parameters used in these algorithms are given in Table 11. As seen from this table, the parameter contributing to the neighbourhood effect is almost same as the previous case and is of low value. Comparing the fuzzy and typicality indices of Table 11 with those of Table 10, it is found that the indices are unchanged. As observed from Fig. 5(g)–(r), the algorithms could segment the image properly and estimate the bias field accurately. Thus, the bias corrected images have also been obtained accurately. This has also been reflected in the misclassification error tabulated in Table 9. Thus, the proposed algorithms such as BCPFCM, BCPNFCM, BCSPNFCM could estimate bias fields of both low and high frequency.

Brain MR images:

Besides synthetic images, the proposed algorithms have also been tested with brain MR images with 40% spatial inhomogeneity (bias field) obtained from the BrainWeb data base (http://brainweb.bic.mni.mcgill.ca/brainweb/) and IBSR database [6]. We have considered both axial and sagittal view of brain MRI images. Fig. 6(a) shows the brain MR image of axial view with 40% bias field and the corresponding ground truth image is shown in Fig. 6(b).

Fig. 6(c) and (d) shows the results obtained by FCM and PFCM algorithms respectively. As observed, in case of FCM, proper segmentation could not be obtained and therefore the misclassification error is as high as 28.34%. Fig. 6(e)–(p) shows the results obtained by the BCFCM algorithm [4] and our proposed BCPFCM, BCPNFCM, BCSPNFCM algorithms. Using the above algorithms the images could be segmented and bias field could also be extracted. As observed from Table 15, the percentage of misclassification error of BCPNFCM algorithm is less than that of BCFCM algorithm.

The corresponding bias corrected images are shown in Fig. 6(g), (j), (m) and (p). The parameters used are tabulated in Table 12, where it can be observed that value of α is 0.09 in case of BCSPNFCM algorithm thereby indicating more contribution of the neighbourhood pixels as compared to other algorithms. In each case, the bias field could be estimated as shown in Fig. 6(f)–(o) and the nonlinearity in the estimated bias fields can also be observed from these figures. As seen from Table 15, the percentage of misclassification error is minimum in case of BCPNFCM algorithm.

While it is known that the addition of noise to the slices will adversely affect segmentation results, nevertheless we have added some noise to the tissue classes from the BrainWeb database to investigate the performance of the proposed algorithms. The noise percentage as defined by BrainWeb Database is as follows. The "percent noise" number represents the percent ratio of the standard deviation of the White Gaussian Noise Versus the signal for the reference. We have considered the T2 images and in these cases the CSF is the reference tissue.

The second example considered is again from the same axial view brain MR image with 40% bias and three different noise conditions such as 1%, 3% and 5% from the BrainWeb database. These images have been shown in Fig. 7(a) and the manually constructed ground truth images have been shown in Fig. 7(b). Fig. 7(c) shows the segmented image obtained by FCM and results obtained by PFCM is shown in Fig. 7(d). As observed, for 1% noise case, the segmentation is not proper and hence the misclassification error is 28.12%. For 3% and 5% noise cases, the errors are 19.17% and 22.26%. Similarly, in case of PFCM algorithm, the error is 21.77% for 1% noise case and 22.69% and 24.87% for 3% and 5% noises, respectively. It may be observed that in case of FCM algorithm the error in noisy case is less than that of noise free case. The errors with noises are expected to increase but this decrease may be attributed to the following reasons. The noise added at a given pixel sometimes cancels the effects of the nonlinearity resulting from bias. Additionally, the objective function does not include the effects of neighboring pixels and hence the net change happens in several individual pixels. This results in the decrease in misclassification error. Therefore, for 1% noise the error (28.12%) is close to that of noise free case (28.34%) and with increase in noise the error reduces because of the probable change of pixels. Similar explanations could be in favor of PFCM algorithm that does not take care of the effect of neighboring pixels. But, in case of BCFCM, BCPFCM, BCPNFCM and BCSPNFCM algorithms, the objective functions have different degree of contributions of neighborhood pixels for achieving segmentation. Therefore, as observed from Table 15, as expected, with increase in noise the errors increase. The noise, on a given pixel, which otherwise would have nullified some effects of the bias field is taken care by the noisy neighborhood pixels. Thus the effect of noise is reflected on the efficacy of segmentation. The segmented

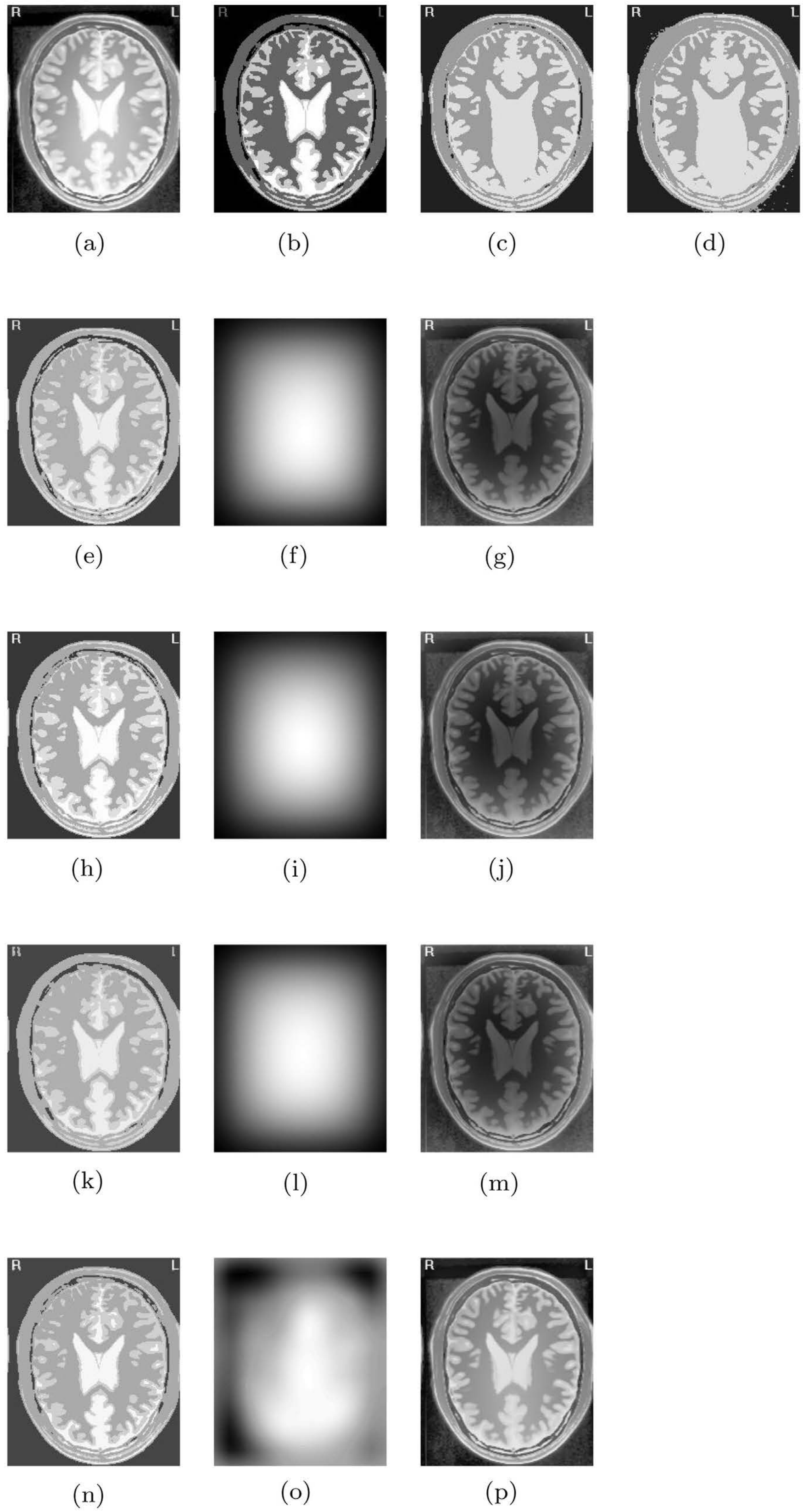

Fig. 6. Segmentation image obtained by different methods and the estimated bias field of brain MR image Axial view with 40% bias. (a) Raw MR image with 40% bias, (b) ground truth image, (c) FCM, (d) PFCM, (e, h, k, n) Segmented results using BCFCM, BCPFCM, BCPNFCM, BCSPNFCM. (f, i, l, o) Estimated bias field using BCFCM, BCPFCM, BCPNFCM, BCSPNFCM. (g, j, m, p) Bias corrected MR image using using BCFCM, BCPFCM, BCPNFCM, BCSPNFCM.

Table 10
Parameter values for low frequency synthetic image with bias.

Algorithms	Weight a	Weight b	Neigh-borhood effect (α)	N_k, $N_c = c - 1$	Fuzzy index (m)	Typi-cality index (n)
BCFCM	–	–	.04	9, –	2	–
BCPFCM	.29	4	.04	9, 1	2	2
BCPNFCM	.18	3.85	.06	9, 1	2	2
BCSPNFCM	.29	4	.04	9, 1	2	2

Table 11
Parameter values for high frequency synthetic image with bias.

Algorithms	Weight a	Weight b	Neigh-borhood effect (α)	N_k, $N_c = c - 1$	Fuzzy index (m)	Typi-cality index (n)
BCFCM	–	–	.04	9, –	2	–
BCPFCM	.29	4	.04	9, 1	2	2
BCPNFCM	.18	9	.04	9, 1	2	2
BCSPNFCM	.7	7	.06	9, 1	2	2

Table 12
Parameter values for raw MR image Axial view with 40% bias.

Algorithms	Weight a	Weight b	Neigh-borhood effect (α)	N_r, $N_c = c - 1$	Fuzzy index (m)	Typi-cality index (n)
BCFCM	–	–	.04	9, –	2	–
BCPFCM	.29	55	.04	9, 3	2	2
BCPNFCM	.29	55	.04	9, 3	2	2
BCSPNFCM	.29	15	.09	9, 3	2	2

images obtained by BCFCM, and our three proposed algorithms are shown in Fig. 7(e)–(h). It may be observed that segmentation could be obtained even with noisy images. The misclassification errors are given in Table 15, where it can be seen that BCPNFCM algorithm produced error of 5.69%, which is the lowest among all the schemes. It may also be observed that for noisy and noise-free cases, BCPNFCM algorithm provided minimum error among all the algorithms. The parameters used are tabulated in Table 13. Thus the BCPNFCM algorithm produced best result among all the algorithms.

The third example considered is the sagittal view of the brain MR image, with 40% bias from the same data base and this is shown in Fig. 8(a). The corresponding ground truth is shown in Fig. 8(b). BCFCM algorithm [4] and the three proposed algorithms have been tested on this data set. Segmented results presented in Fig. 8(e)–(g) correspond to the BCFCM algorithm, where it may be observed that there are three classes in segmented image. The estimated bias field is shown in 8(f) while Fig. 8(g) shows the bias corrected image. The parameters used for BCFCM are given in Table 14, where it can be observed that α has been kept low at value of 0.04, thereby

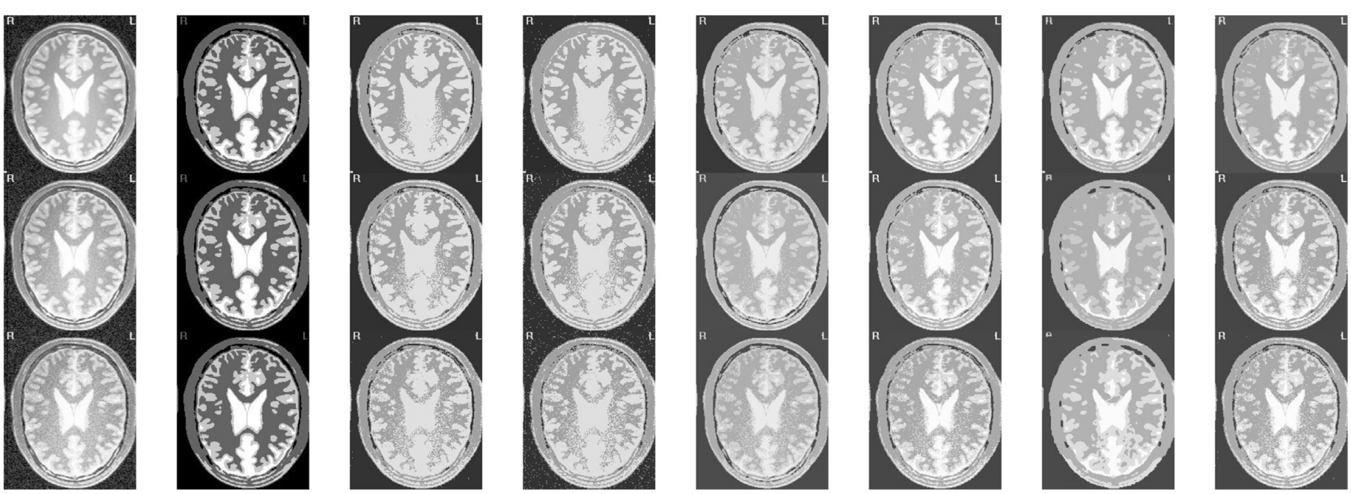

(a) (b) (c) (d) (e) (f) (g) (h)

Fig. 7. Segmented images with different techniques: (a) Axial Raw MR image with noise (images with 1%, 3% and 5% noise and 40% bias from first row to third row of the first column), (b) ground truth, segmentation results by (c) FCM, (d) PFCM, (e) BCFCM, (f) BCPFCM, (g) BCPNFCM, (h) BCSPNFCM.

Table 13
Parameter values for Raw MR image Axial view with 40% bias and noise.

Algorithms	Weight a	Weight b	Neigh-borhood effect (α)	N_r, $N_c = c - 1$	Fuzzy index (m)	Typi-cality index (n)
BCFCM	–	–	.04	9, –	2	–
BCPFCM	.29	55	.04	9, 3	2	2
BCPNFCM	.29	55	.04	9, 3	2	2
BCSPNFCM	.29	25	.17	9, 3	2	2

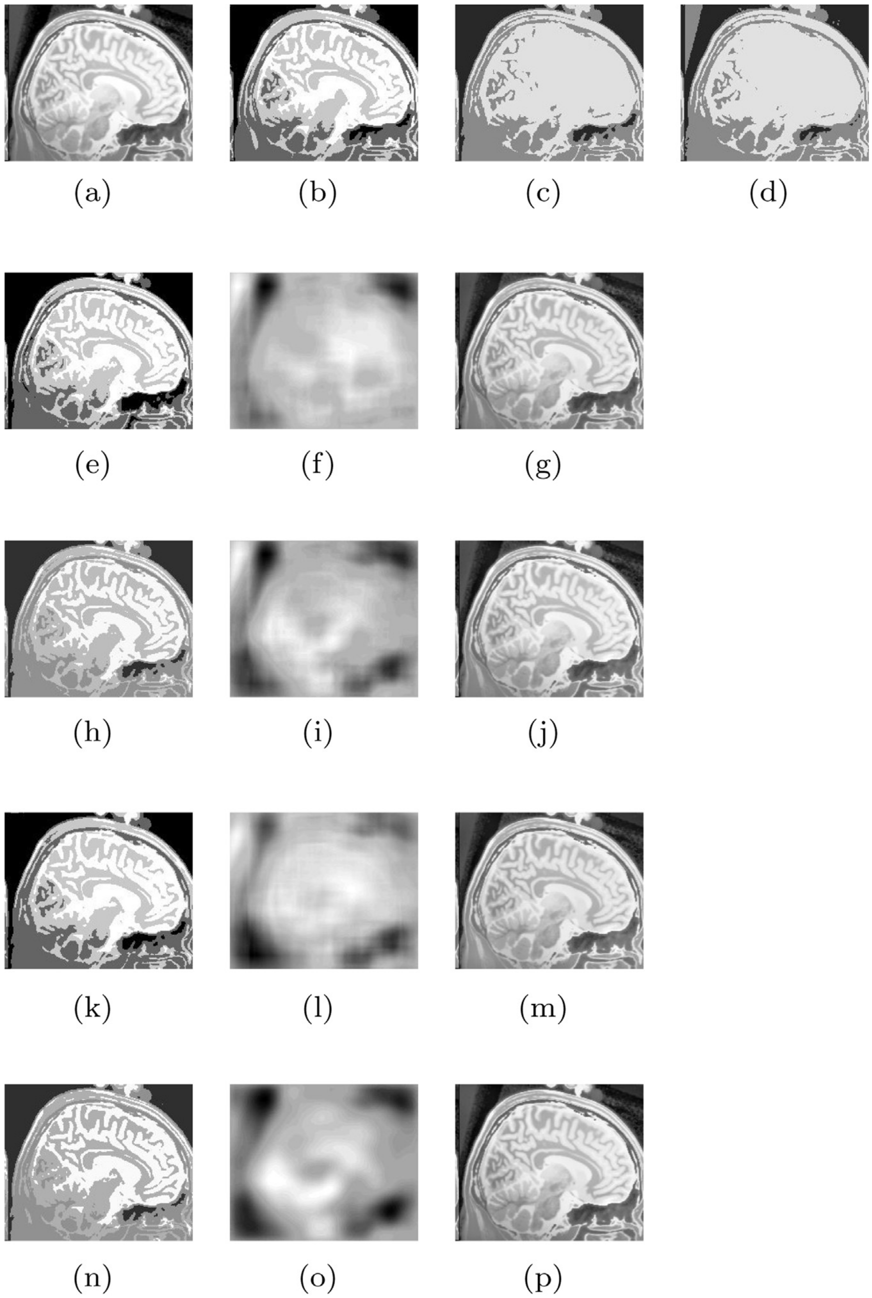

Fig. 8. Segmentation result, estimated bias field and the bias corrected images of (a) Raw MR image sagittal view of brain with 40% bias, (b) ground truth image, (c) FCM, (d) PFCM, (e, h, k, n) segmented results using BCFCM, BCPFCM, BCPNFCM, BCSPNFCM. (f, i, l, o) Estimated bias field using BCFCM, BCPFCM, BCPNFCM, BCSPNFCM. (g, j, m, p) Bias corrected MR image using BCFCM, BCPFCM, BCPNFCM, BCSPNFCM.

indicating the minor effect of the neighbourhood pixels. The neighboring pixels have been confined to (3×3) neighbourhood. The misclassification error is 8.3% and is tabulated in Table 16. Fig. 8(h)–(p) shows the segmented images, estimated bias field, and bias corrected images obtained by the proposed BCPFCM, BCPNFCM, BCSPNFCM algorithms.

In all the cases, the bias fields have been estimated and the percentage of misclassification is lower than that of BCFCM algorithm

Table 14
Parameter values for Raw MR image sagittal view of brain with 40% bias.

Algorithms	Weight a	Weight b	Neigh-borhood effect (α)	N_r, $N_c = c - 1$	Fuzzy index (m)	Typi-cality index (n)
BCFCM	–	–	.04	9, –	2	–
BCPFCM	.29	21	.06	9, 3	2	2
BCPNFCM	.29	38	.04	9, 3	2	2
BCSPNFCM	.29	55	.06	9, 3	2	2

Fig. 9. Segmentation of Axial volume from BrainWeb database. (a) Original image, slice 91, 92, 94, 95, 96, 97, 98, 100 arranged in the ascending order from top row to bottom row of the first column, (b) ground truth, (c) BCFCM. (d) BCPFCM, (e) BCPNFCM, (f) BCSPNFCM.

except BCPNFCM algorithm. The performance of the proposed algorithms have been found to be better than that of FCM and also BCFCM algorithms.

In order to validate the consistency of the performance of the algorithm, we have applied the proposed algorithms and also Ahmed et al.'s [4] algorithm on 8 slices numbered from 91 to 100 from BrainWeb database as shown in Fig. 9(a) and corresponding ground truth images are shown in Fig. 9(b). The results obtained by Ahmed et al.'s BCFCM algorithm is shown in Fig. 9(c). The results obtained by the three proposed algorithms are shown in Fig. 9(d), (e) and (f). The misclassification error resulting from our proposed algorithms and Ahmed et al.'s algorithm for the 8 different slices

Table 15
Mis-classification error for raw MR images Axial view with 40% bias.

Algorithm	Mis-classification error raw MR image	Mis-classification error raw MR image with noise			Simulation time (in s)
		1%	3%	5%	
FCM	28.34	28.12	19.17	22.26	3
PFCM	23.14	21.77	22.69	24.87	6
BCFCM	6.91	7.72	11.84	16.16	9
BCPFCM	6.47	7.55	10.08	14.63	6
BCPNFCM	2.91	5.69	8.35	11.92	5
BCSPNFCM	6.33	7.40	11.48	14.12	10

Table 16
Mis-classification error for raw MR image sagittal view of brain with 40% bias.

Algorithms	Mis-classification error raw MR image (%)
FCM	35.31
PFCM	34.68
BCFCM	8.30
BCPFCM	7.91
BCPNFCM	9.78
BCSPNFCM	7.76

Table 17
Mis-classification error for raw MR image Axial view of brain with 40% bias.

Algorithms ↓ Slice No. →	91	92	94	95	96	97	98	100
BCFCM	9.99	10.55	10.14	11.49	11.63	10.88	10.40	10.69
BCPFCM	10.17	10.54	9.90	11.16	10.68	10.19	9.64	10.77
BCPNFCM	5.85	7.55	7.14	8.07	7.33	6	4.71	5.85
BCSPNFCM	10.50	10.76	10.54	11.29	11.26	10.58	10	10.91

Table 18
Error statistics for raw MR image Axial view of brain with 40% bias of Table 17.

Algorithms	Mean	Variance
BCFCM	10.72	.34
BCPFCM	10.38	.24
BCPNFCM	6.56	1.27
BCSPNFCM	10.73	.18

have been shown in Table 17 and the error variances have been found to be low as presented in Table 18. Thus the performance of the algorithm has been found to be consistent when tested with MR image set.

The performance of the proposed algorithms was compared with other algorithms on six slices taken from IBSR database and are shown in Fig. 10(a). These slices are the same slices on which Ortiz et al. [29] have tested their algorithms. They have compared the performance based on Tanimoto's index [29] and we have also compared with the same index which is given as:

$$T(S1, S2) = \frac{|S1 \cap S2|}{|S1 \cup S2|}$$

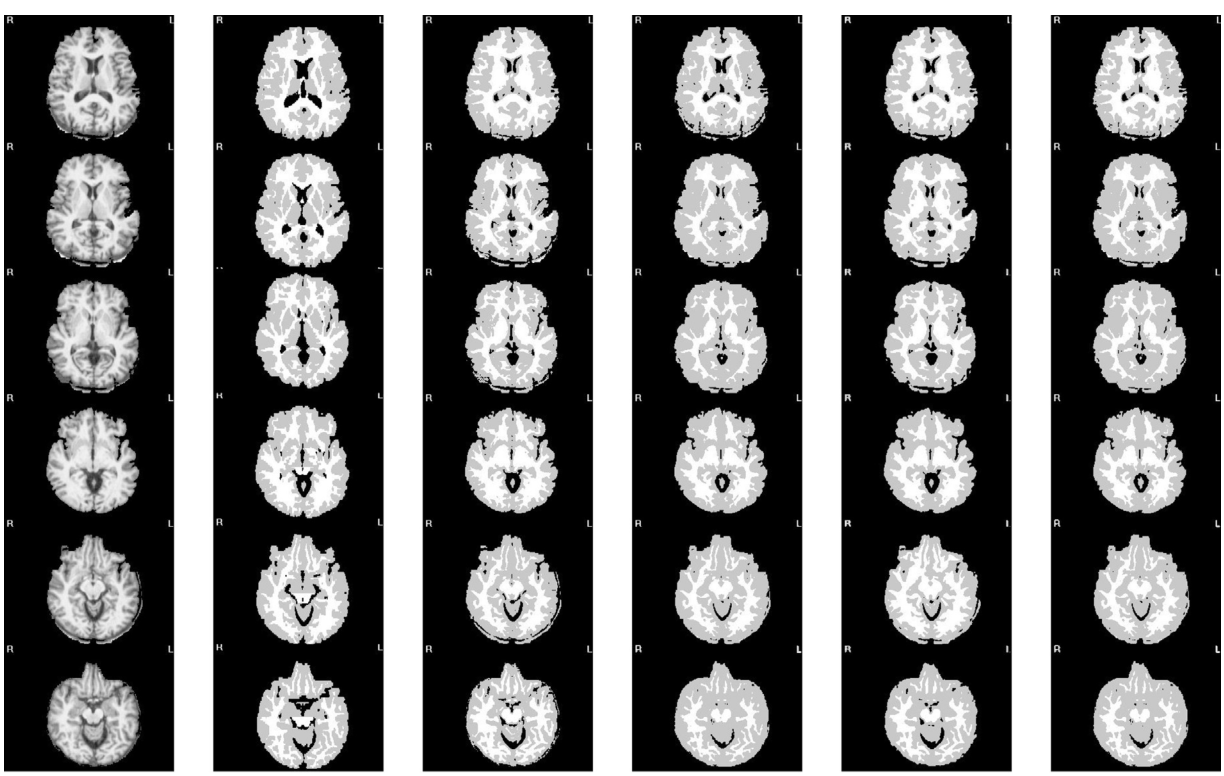

(a) (b) (c) (d) (e) (f)

Fig. 10. Segmentation of Axial volume from IBSR Database. (a) Original image, slice 115, 120, 125, 130, 135, 139 arranged in the ascending order from top row to bottom row of the first column, (b) ground truth, (c) BCFCM, (d) BCPFCM, (e) BCPNFCM, (f) BCSPNFCM.

Table 19
Mean and standard deviation of Tanimoto's index.

Algorithms	Reference	WM index	GM index	CSF index
EGS-SOM	[29,6]	0.70 ± 0.04	0.70 ± 0.04	0.22 ± 0.08
Constrained GMM	[30,6]	0.68 ± 0.04	0.66 ± 0.06	.20 ± 0.06
HFS-SOM	[29,6]	0.60 ± 0.1	0.60 ± 0.15	0.1 ± 0.05
Adaptive MAP(amap)	[30,6]	0.57 ± 0.13	0.58 ± 0.17	0.07 ± 0.03
Biased MAP(bmap)	[30,6]	0.56 ± 0.17	0.58 ± 0.21	0.07 ± 0.03
Maximum a posteriori probability (map)	[30,6]	0.47 ± 0.11	0.57 ± 0.20	0.07 ± 0.03
Tree-structure *k*-means (tskmeans)	[30,6]	0.48 ± 0.12	0.58 ± 0.19	0.05 ± 0.02
Maximum likelihood (mlc)	[30,6]	0.54 ± 0.16	0.57 ± 0.20	0.06 ± 0.03
BCFCM		0.44 ± 0.04	0.56 ± 0.02	0.27 ± 0.13
BCPFCM		0.42 ± 0.04	0.60 ± 0.04	0.19 ± 0.11
BCPNFCM		0.43 ± 0.04	0.56 ± 0.02	0.26 ± 0.14
BCSPNFCM		0.38 ± 0.11	0.58 ± 0.04	0.20 ± 0.11

where S1 is the segmentation set and S2 is the ground truth. The index for White Matter (WM), Gray Matter (GM) and Cerebro Spinal Fluid (CSF) tissue classes for different algorithms have been shown in Table 19. The indices in 3–5th column of Table 19 indicate the mean and standard deviation obtained for different tissue classes, White Matter, Gray Matter and Cerebro Spinal Fluid. The mean and standard deviation obtained by our proposed algorithms are comparable to those of the state of the art algorithms. In some cases the standard deviations obtained by our proposed algorithms are lower than those of others. For example, in case of Gray Matter(GM) the standard deviation obtained by BCPNFCM algorithm is 0.02 where as for HFS-SOM and constrained GMM are 0.15 and 0.21, respectively. Therefore, the performance of the proposed algorithms are comparable to those of the state of the art algorithms as given by the cited references in Table 19.

9. Conclusions

Estimation of bias field and thereby obtaining bias corrected images is the focus of this research, specifically with bias. Attempts have been made to propose novel schemes for simultaneous estimation of bias field and obtaining segmentation of brain MR images. In this regard, BCFCM algorithm has been proposed by Ahmed et al. [4], but we have proposed some improvement at this font. The notion behind the schemes is to jointly consider the typicality as well as the fuzzy membership measures to model the bias field and noise. The isolated points or noise have been taken care by differently weighing the above two memberships. We have also considered the fuzzy and typicality measures of the neighbourhood pixels together with the pixel under consideration. This has helped to model the slowly varying bias field with noise. The effect of neighbourhood pixels could be controlled through different parameters. In this process, we have also incorporated the local and global effect of fuzzy memberships and typicality, thus reinforcing the model to take care of noises. The proposed algorithms have been successfully tested on synthetic as well as brain MR images. The initial values of cluster centers for our different algorithms are not same rather they are different and are expected to evolve to eventually converge to the final cluster centers. The performance of the proposed algorithms has been found to be better than that of BCFCM [4] in terms of misclassification error. The only bottleneck of these algorithms is that the parameters have been selected on trial and error. Current research work focuses on estimation of these parameters together with the prototypes.

Acknowledgment

The authors gratefully acknowledge the research facilities provided by Siksha 'O' Anusandhan University, India.

Appendix A. BCPFCM

$$J'_{\mathrm{BCPFCM}} = J_{\mathrm{BCPFCM}} + \sum_{j=1}^{p} \lambda \left(1 - \sum_{i=1}^{c} u_{ij}\right)$$

$$\begin{aligned} J'_{\mathrm{BCPFCM}} = & \sum_{i=1}^{c}\sum_{j=1}^{p} (a u_{ij}^{m} + b t_{ij}^{n}) \|y_j - \beta_j - v_i\|^2 \\ & + \frac{\alpha}{N_r} \sum_{i=1}^{c}\sum_{j=1}^{p} \left(a u_{ij}^{m} + b t_{ij}^{n}\right) \left(\sum_{y_r \in N_k} \|y_r - \beta_r - v_i\|^2\right) \\ & + \sum_{i=1}^{c} \eta_i \sum_{j=1}^{p} (1 - t_{ij})^{n} + \sum_{j=1}^{p} \lambda \left(1 - \sum_{i=1}^{c} u_{ij}\right) \end{aligned} \tag{A.1}$$

$$\frac{\partial J'_{\mathrm{BCPFCM}}}{\partial u_{ij}} = 0$$

$$\frac{\partial J'_{\mathrm{BCPFCM}}}{\partial u_{ij}} = m\, a\, u_{ij}^{m-1} D_{ij} + m\, a\, \frac{\alpha}{N_r}\, u_{ij}^{m-1} \gamma_i - \lambda = 0 \tag{A.2}$$

where $D_{ij} = \|y_j - \beta_j - v_i\|^2$ and $\gamma_i = \sum_{y_r \in N_k} \|y_r - \beta_r - v_i\|^2$

$$u_{ij} = \left[\frac{\lambda}{a\, m \left(D_{ij} + \frac{\alpha}{N_r} \gamma_i\right)}\right]^{\left(\frac{1}{m-1}\right)} \tag{A.3}$$

$$\sum_{k=1}^{c} u_{kj} = 1 \tag{A.4}$$

$$\sum_{k=1}^{c} \left[\frac{\lambda}{a\, m \left(D_{kj} + \frac{\alpha}{N_r} \gamma_k\right)}\right]^{\left(\frac{1}{m-1}\right)} = 1 \tag{A.5}$$

$$\lambda = \frac{a\, m}{\left(\sum_{k=1}^{c} \left(\frac{1}{D_{kj} + \frac{\alpha}{N_r}\gamma_k}\right)^{\frac{1}{m-1}}\right)^{m-1}} \tag{A.6}$$

Applying the value of λ in (A.3), we get the update equation for fuzzy membership,

$$u_{ij} = \frac{1}{\sum_{k=1}^{c} \left(\frac{D_{ij} + \frac{\alpha}{N_r}\gamma_i}{D_{kj} + \frac{\alpha}{N_r}\gamma_k}\right)^{\frac{1}{m-1}}} \tag{A.7}$$

Taking the derivative of J'_{BCPFCM} with respect to t_{ij} the update function for cluster prototype is obtained.

$$\frac{\partial J'_{BCPFCM}}{\partial t_{ij}} = b\, n\, t_{ij}^{n-1} D_{ij} + \frac{\alpha}{N_r} b\, n\, t_{ij}^{n-1}\, \gamma_i - n\, \eta_i \left(1 - t_{ij}\right)^{n-1} = 0 \quad \text{(A.8)}$$

$$t_{ij} = \frac{1}{1 + \left[\frac{b}{\eta_i}(D_{ij} + \frac{\alpha}{N_r}\gamma_i)\right]^{\frac{1}{n-1}}} \quad \text{(A.9)}$$

The update equation for cluster prototype is obtained by taking derivative of J'_{BCPFCM} with respect to v_i

$$\frac{\partial J'_{BCPFCM}}{\partial v_i} = \sum_{j=1}^{p} \left(a u_{ij}^m + b\, t_{ij}^n\right)(y_j - \beta_j - v_i) + \frac{\alpha}{N_r} \sum_{j=1}^{p} \left(a\, u_{ij}^m + b\, t_{ij}^n\right) \times \sum_{y_r \in N_k} \left(y_r - \beta_r - v_i\right) = 0 \quad \text{(A.10)}$$

Solving (A.10) for v_i, we get

$$v_i = \frac{\sum_{j=1}^{p}(a u_{ij}^m + b t_{ij}^n)\|y_j - \beta_j\| + \frac{\alpha}{N_r}\sum_{j=1}^{p}(a u_{ij}^m + b t_{ij}^n)\sum_{y_r \in N_k}(y_r - \beta_r)}{\sum_{j=1}^{p}(a u_{ij}^m + b t_{ij}^n) + \alpha \sum_{j=1}^{p}(a u_{ij}^m + b t_{ij}^n)} \quad \text{(A.11)}$$

The update equation for bias field is obtained by solving J'_{BCPFCM} with respect to β_j.

$$\frac{\partial J'_{BCPFCM}}{\partial \beta_i} = \sum_{i=1}^{c} \left(a\, u_{ij}^m + b\, t_{ij}^n\right) \left(y_j - \beta_j - v_i\right) = 0 \quad \text{(A.12)}$$

$$\beta_j = y_j - \frac{\sum_{i=1}^{c}(a u_{ij}^m + b t_{ij}^n) v_i}{\sum_{i=1}^{c}(a u_{ij}^m + b t_{ij}^n)} \quad \text{(A.13)}$$

References

[1] J.C. Bezdek, R. Ehrlich, W. Full, FCM: The fuzzy c-means clustering algorithm, Comput. Geosci. 10 (2–3) (1984) 191–203.
[2] R. Krishnapuram, J.M. Keller, A possibilistic approach to clustering, IEEE Trans. Fuzzy Syst. 1 (2) (1993) 98–110.
[3] N.R. Pal, K. Pal, J.M. Keller, J.C. Bezdek, A possibilistic fuzzy c-means clustering algorithm, IEEE Trans. Fuzzy Syst. 13 (4) (2005) 517–530.
[4] M.N. Ahmed, S.M. Yamany, N. Mohamed, A.A. Farag, A modified fuzzy c-means algorithm for bias field estimation and segmentation of MRI data, IEEE Trans. Med. Imaging 21 (3) (2002) 193–199.
[5] J. Aparajeeta, P.K. Nanda, N. Das, Bias field estimation and segmentation of MR image using modified fuzzy-C means algorithms, in: Proceedings of Eighth International Conference on Advances in Pattern Recognition (ICAPR), IEEE, 2015, pp. 1–6.
[6] Internet Brain Segmentation Repository, Neuroinformatics tools and resources, https://www.nitrc.org/frs/?group_id=48.
[7] D.L. Pham, J.L. Prince, Adaptive fuzzy segmentation of magnetic resonance images, IEEE Trans. Med. Imaging 18 (9) (1999) 737–751.
[8] D.L. Pham, Spatial models for fuzzy clustering, Comput. Vision Image Understand. 84 (2) (2001) 285–295.
[9] B. Belaroussi, J. Milles, S. Carme, Y.M. Zhu, H. Benoit-Cattin, Intensity non-uniformity correction in MRI: existing methods and their validation, Med. Image Anal. 10 (2) (2006) 234–246.
[10] F. Zhao, L. Jiao, H. Liu, Fuzzy c-means clustering with non local spatial information for noisy image segmentation, Front. Comput. Sci. China 5 (1) (2011) 45–56.
[11] L. Szilagy, Z. Benyo, S.M. Szilagyi, H.S. Adam, MR brain image segmentation using an enhanced fuzzy c-means algorithm, in: Proceedings of IEEE 25th International Conference on Engineering in Medicine and Biology Society (EMBS), IEEE, 2003, pp. 724–726.
[12] A. Liew, H. Yan, An adaptive spatial fuzzy clustering algorithm for 3-d MR image segmentation, IEEE Trans. Med. Imaging 22 (9) (2003) 1063–1075.
[13] S. Chen, D. Zhang, Robust image segmentation using FCM with spatial constraints based on new kernel-induced distance measure, IEEE Trans. Syst. Man Cybern. B: Cybern. 34 (4) (2004) 1907–1916.
[14] L. Liao, T. Lin, B. Li, MRI brain image segmentation and bias field correction based on fast spatially constrained kernel clustering approach, Pattern Recognit. Lett. 29 (10) (2008) 1580–1588.
[15] L. Chen, C. Chen, M. Lu, A multiple-kernel fuzzy C-means algorithm for image segmentation, IEEE Trans. Syst. Man Cybern. B: Cybern. 41 (5) (2011) 1263–1274.
[16] R. Xu, J. Ohya, An improved kernel-based fuzzy c-means algorithm with spatial information for brain MR image segmentation, in: Proceedings of IEEE 25th International Conference on Image and Vision Computing New Zealand (IVCNZ), IEEE, 2010, pp. 1–7.
[17] S. Shen, W.A. Sandham, M.H. Granat, A. Sterr, Intensity non-uniformity correction of magnetic resonance images using a fuzzy segmentation algorithm, in: Proceedings of IEEE 27th International Conference on Engineering in Medicine and Biology Society (EMBS), IEEE, 2005, pp. 3035–3038.
[18] J. Wang, J. Kong, Y. Lu, M. Qi, B. Zhang, A modified FCM algorithm for MRI brain image segmentation using both local and non-local spatial constraints, Comput. Med. Imaging Graph. 32 (8) (2008) 685–698.
[19] O. Salvado, D.L. Wilson, Entropy based method to correct intensity inhomogeneity in MR images, in: Proceedings of IEEE 26th International Conference on Engineering in Medicine and Biology Society (EMBS), IEEE, 2004, pp. 164–167.
[20] J. Luo, Y. Zhu, P. Clarysse, I. Magnin, Correction of bias field in MR images using singularity function analysis, IEEE Trans. Med. Imaging 24 (8) (2005) 1067–1085.
[21] M. Siyal, L. Yu, An intelligent modified fuzzy c-means based algorithm for bias estimation and segmentation of brain MRI, Pattern Recognit. Lett. 26 (13) (2005) 2052–2062.
[22] L. Szilagyi, S.M. Szilagyi, Z. Benyo, Efficient feature extraction for fast segmentation of MR brain images, in: Proceedings of LNCS, Image Analysis, vol. 4522, 2007, pp. 611–620.
[23] L. Szilagyi, S.M. Szilagyi, Z. Benyo, A modified fuzzy c-means algorithm for MR brain image segmentation, in: Proceedings of LNCS, Image Analysis and Recognition, vol. 4633, 2007, pp. 866–877.
[24] J.V. Manjon, J.J. Lull, J.C. Caballero, G.G. Marti, L.M. Bonmati, M. Robles, A nonparametric MRI inhomogeneity correction method, Med. Image Anal. 11 (4) (2007) 336–345.
[25] J. Milles, Y.M. Zhu, G. Gimenez, C.R. Guttmann, I.E. Magnin, MRI intensity nonuniformity correction using simultaneously spatial and gray-level histogram information, Comput. Med. Imaging Graph. 31 (2) (2007) 81–90.
[26] N. Verma, M.C. Cowperthwaite, M.K. Markey, Variational level set approach for automatic correction of multiplicative and additive intensity inhomogeneities in brain MR images, in: Proceedings of IEEE 34th International Conference on Engineering in Medicine and Biology Society (EMBS), IEEE, 2012, pp. 98–101.
[27] Z.X. Ji, Q.S. Sun, D.S. Xia, A modified possibilistic fuzzy c-means clustering algorithm for bias field estimation and segmentation of brain MR image, Comput. Med. Imaging Graph. 35 (5) (2011) 383–397.
[28] L. Szilagyi, S.M. Szilagyi, B. Benyo, Z. Benyo, Intensity inhomogeneity compensation and segmentation of MR brain images using hybrid c-means clustering models, Biomed. Signal Process. Control 6 (1) (2011) 3–12.
[29] A. Ortiz, J. Gorriz, J. Ramirez, D. Salas-Gonzalez, J. Llamas-Elvira, Two fully-unsupervised methods for MR brain image segmentation using SOM-based strategies, Appl. Soft Comput. 13 (5) (2013) 2668–2682.
[30] H. Greenspan, A. Ruf, J. Goldberger, Constrained Gaussian mixture model framework for automatic segmentation of MR brain images, IEEE Trans. Med. Imaging 25 (9) (2006) 1233–1245.